J|A|C|S
ARTICLES
Published on Web 06/18/2003

# Alternating Oligo(*p*-phenylene vinylene)−Perylene Bisimide Copolymers: Synthesis, Photophysics, and Photovoltaic Properties of a New Class of Donor−Acceptor Materials

Edda E. Neuteboom,[†] Stefan C. J. Meskers,[†] Paul A. van Hal,[†] Jeroen K. J. van Duren,[†] E. W. Meijer,[†] René A. J. Janssen,*[,†] Hélène Dupin,[‡] Geoffrey Pourtois,[‡] Jérôme Cornil,[‡,§] Roberto Lazzaroni,[‡,§] Jean-Luc Brédas,[‡,§] and David Beljonne[‡,§]

*Contribution from the Laboratory of Macromolecular and Organic Chemistry, Eindhoven University of Technology, P.O. Box 513 5600 MB Eindhoven, The Netherlands Chemistry of Novel Materials, University of Mons-Hainaut, Place du Parc 20, 7000 Mons, Belgium, and Department of Chemistry, The University of Arizona, Tucson, Arizona 85721*

Received February 28, 2003; E-mail: r.a.j.janssen@tue.nl

***Abstract:*** A Suzuki polycondensation reaction has been used to synthesize two copolymers consisting of alternating oligo(*p*-phenylene vinylene) (OPV) donor and perylene bisimide (PERY) acceptor chromophores. The copolymers differ by the length of the saturated spacer that connects the OPV and PERY units. Photoinduced singlet energy transfer and photoinduced charge separation in these polychromophores have been studied in solution and in the solid state via photoluminescence and femtosecond pump−probe spectroscopy. In both polymers a photoinduced electron transfer occurs within a few picoseconds after excitation of the OPV or the PERY chromophore. The electron transfer from OPV excited state competes with a singlet energy transfer state to the PERY chromophore. The differences in rate constants for the electron- and energy-transfer processes are discussed on the basis of correlated quantum-chemical calculations and in terms of conformational preferences and folding of the two polymers. In solution, the lifetime of the charge-separated state is longer than in the films where geminate recombination is much faster. However, in the films some charges are able to escape from geminate recombination and diffuse away and can be collected at the electrodes when the polymers are incorporated in a photovoltaic device.

## Introduction

Photoinduced energy and electron transfer between photoactive and electroactive donor (D) and acceptor (A) moieties continues to be an extremely active area of research.[1−6] Numerous photophysical studies of organic D−A molecules have been performed to elucidate and control resonant energy transfer, charge separation, and recombination and to assess the role of intermediates in the deactivation of the initially excited states. The intriguing photophysical and photochemical processes that take place in the natural photosynthetic reaction center have stimulated efforts to design and create artificial donor−acceptor architectures in an attempt to mimic the conversion of light into chemical energy or to create electrical power directly.

Photoinduced electron transfer between donor and acceptor materials is also the initial step in organic and polymer solar cells. In these cells excitations, created by the absorption of light, must be able to diffuse to the interface between the two materials where charge generation can occur. However, the exciton diffusion length in organic and polymer materials is often limited to about 10 nm. This implies that an intimate, nanoscopic, mixing of donor and acceptor is favorable for charge creation. Following this principle, the bulk-heterojunction cell, in which a spontaneous phase separation of the two components into a disordered blend is used to create a large interface, has become one of the most promising concepts in the field of polymer solar cells and resulted in external quantum efficiencies of more than 50% at the absorption maximum.[7−9] A further increase of performance is expected by designing materials that have an improved overlap of their absorption spectrum with the terrestrial solar radiation, especially in the near-infrared region.

A general drawback of the bulk-heterojunction is the fact that the transport and collection of charges in a disordered nanoscale

[†] Eindhoven University of Technology.
[‡] University of Mons-Hainaut.
[§] The University of Arizona.

(1) Kavarnos, G. J. *Fundamentals of Photoinduced Electron Transfer*; Wiley-VCH: Weinheim, 1993.
(2) *Electron Transfer in Chemistry*; Balzani, V., Ed.; Wiley-VCH: Weinheim, 2001; Vols. 1−5.
(3) *Photoinduced Electron Transfer*; Fox, M. A., Chanon, M., Eds.; Elsevier: Amsterdam, 1988; Vols. 1−4.
(4) Warman, J. M.; De Haas, M. P.; Verhoeven, J. W.; Paddon-Row, M. N. *Adv. Chem. Phys.* **1999**, *106*, 571.
(5) Wasielewski, M. R. *Chem. Rev.* **1992**, *92*, 435.
(6) Guldi, D. M. *Chem. Soc. Rev.* **2002**, *31*, 22.
(7) Halls, J. J. M.; Walsh, C. A.; Greenham, N. C.; Marseglia, E. A.; Friend, R. H.; Moratti, S. C.; Holmes, A. B. *Nature* **1995**, *376*, 498.
(8) Yu, G.; Gao, J.; Hummelen, J. C.; Wudl, F.; Heeger, A. J. *Science* **1995**, *270*, 1789.

10.1021/ja034926t CCC: $25.00 

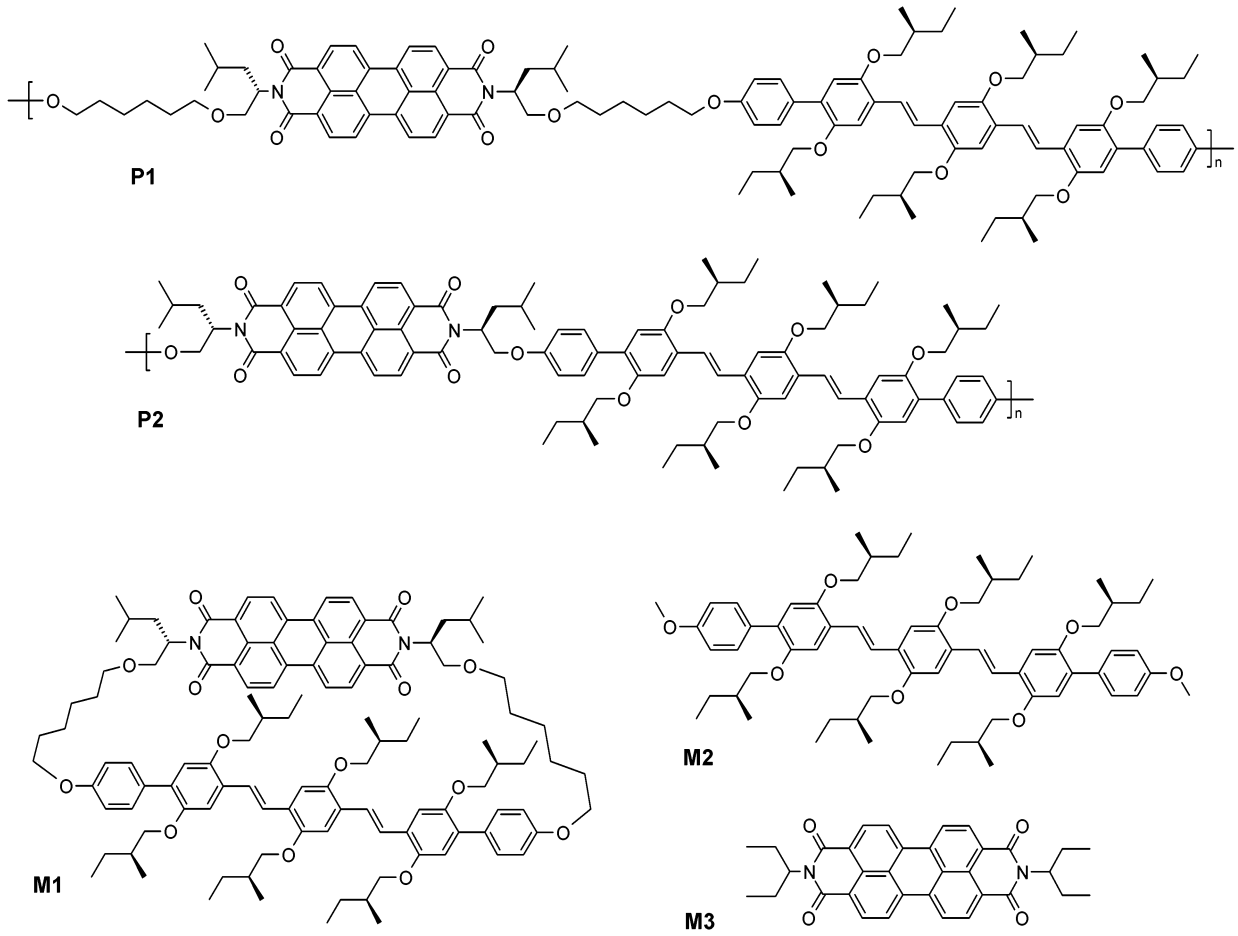


***Figure 1.*** Structure of oligo(*p*-phenylene vinylene)−perylene bisimide alternating copolymers **P1** and **P2** and their model compounds **M1**, **M2**, and **M3**.

blend can be hindered by phase boundaries and discontinuities such as spherical objects and cul-de-sacs. Therefore, the extent, the characteristic dimension, and the contours of the phase separation in polymer−polymer or polymer−molecule blends are essential parameters of bulk-heterojunction solar cells. The actual morphology depends, among others, on details of the preparation procedure (e.g., solvent, temperature, drying speed, substrate). The as-prepared morphology is likely to be kinetically determined rather than thermodynamically stable and subject to further reorganization in time or with temperature.

One way to overcome these drawbacks is by covalently linking the donor and acceptor in a single polymer chain. The covalent bond enables a predefined control over the characteristic distance between donor and acceptor and thereby the extent of phase separation. Two types of covalently linked donor−acceptor polymers have recently come to the attention. The first consists of semiconducting polymers as a donor with pendant acceptor groups,[10−15] while the second has extended donor and acceptor units arranged in a diblock copolymer.[16,17] The latter strategy may have important advantages because the intrinsic tendency of each segment in block copolymers to aggregate in an individual phase provides a means to create a well-ordered nanoscale morphology (e.g., spheres, cylinders, lamellae), governed by the relative volume fractions. While this principle has been utilized in various engineering materials to create fascinating architectures, the use of block copolymers in functional, conjugated polymers has received limited attention.[18−22]

Both oligo(*p*-phenylene vinylene) (OPV)[10,16,23−26] and perylene bisimide (PERY)[27−31] chromophores have been utilized in bulk-heterojunction-like solar cell configurations as donor and as acceptor materials, but their combination has received little attention. In this contribution we present the synthesis and properties of a new class of donor−acceptor polymers, repre-

(9) Brabec, C. J.; Sariciftci, N. S.; Hummelen, J. C. *Adv. Funct. Mater*. **2001**, *11*, 15.
(10) Marcos Ramos, A.; Rispens, M. T.; Van Duren, J. K. J.; Hummelen, J. C.; Janssen, R. A. J. *J. Am. Chem. Soc*. **2001**, *123*, 6714.
(11) Zerza, G.; Cravino, A.; Neugebauer, H.; Sariciftci, N. S.; Gomez, R.; Segura, J. L.; Martin, N.; Svensson, M.; Andersson, M. R. *J. Phys. Chem. A* **2001**, *105*, 4172.
(12) Cravino, A.; Zerza, G.; Neugebauer, H.; Sariciftci, N. S.; Maggini, M.; Bucella, S.; Svensson, M.; Andersson, M. R. *Chem. Commun*. **2000**, 2487.
(13) Zhang, F.; Svensson, M.; Andersson, M. R.; Maggini, M.; Bucella, S.; Menna, E.; Inganäs, O. *Adv. Mater*. **2001**, *13*, 1871.
(14) Wang, S.; Yang, J. Li, Y.; Lin, H. Guo, H.; Xiao, S.; Shi, Z.; Zhu, D.; Woo. H.-S.; Caroll, D. L.; Kee, I.-S.; Lee, J.-H. *Appl. Phys. Lett*. **2002**, *80*, 3847.
(15) Russel, D. M.; Arias, A. C.; Friend, R. H.; Silva, C.; Ego, C.; Grimsdale, A. C.; Müllen, K. *Appl. Phys. Lett*. **2002**, *80*, 2204.
(16) De Boer, B.; Stalmach, U.; Van Hutten, P. F.; Melzer, C.; Krasnikov, V. V.; Hadziioannou, G. *Polymer* **2001**, *42*, 9097.
(17) Stalmach, U.; De Boer, B.; Videlot, C.; Van Hutten, P. F.; Hadziioannou, G. *J. Am. Chem. Soc*. **2000**, *122*, 5464.
(18) Hempenius, M. A.; Langeveld-Voss, B. M. W.; van Haare, J. A. E. H.; Janssen, R. A. J.; Sheiko, S. S.; Spatz, J. P.; Möller, M.; Meijer, E. W. *J. Am. Chem. Soc*. **1998**, *120*, 2798.
(19) Liu, J.; Sheina, E.; Kowalewski, T.; McCullough, R. D. *Angew. Chem., Int. Ed*. **2002**, *41*, 329.
(20) Wang, H.; Wang, H. H.; Urban, V. S.; Littrell, K. C.; Thiyagarajan, P.; Yu, L. *J. Am. Chem. Soc*. **2000**, *122*, 6855.
(21) Malenfant, P. R. L.; Groenendaal, L.; Fréchet, J. M. J. *J. Am. Chem. Soc*. **1998**, *120*, 10990.
(22) Wang, H.; Ng, M.-K.; Wang, L. Yu, L.; Lin, B.; Meron, M.; Xiao, Y. *Chem. Eur. J*. **2002**, *8*, 3246.

***Scheme 1.*** Synthesis of the Perylene Bisimide Monomer **6**[a]

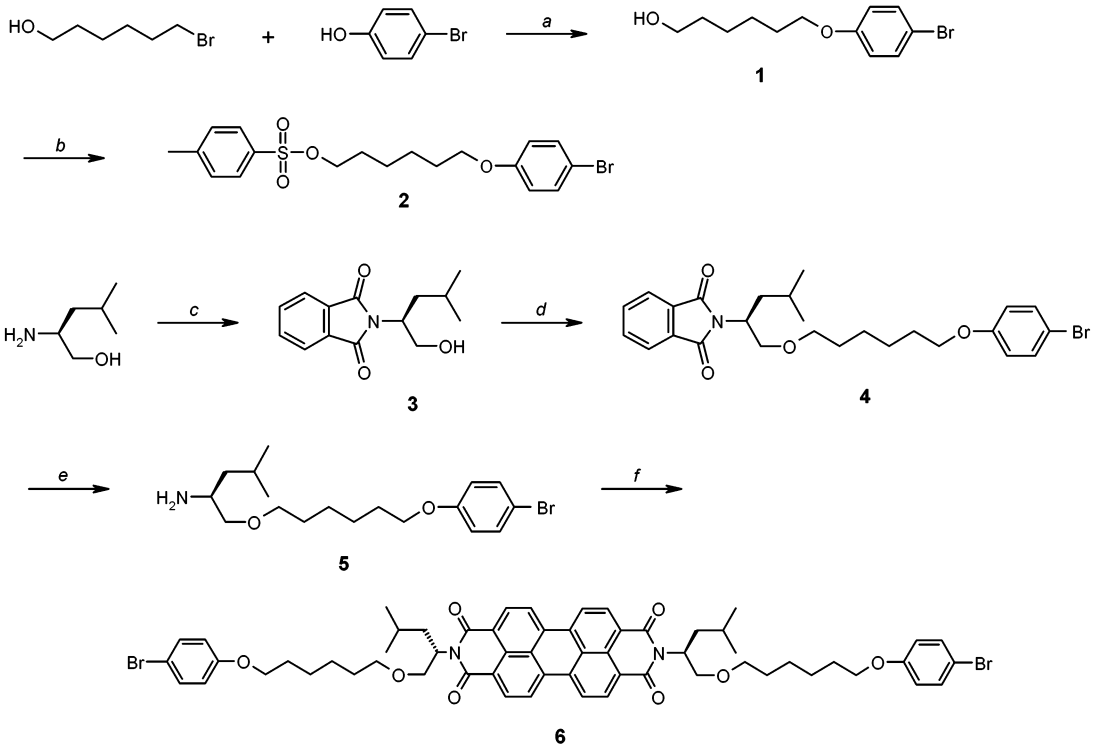


[a] (a) $K_2CO_3$, TBAB, acetone, reflux, 91%; (b) TosCl, pyridine, 4 °C, 75%; (c) phthalic anhydride, toluene, reflux, 94%; (d) **2**, potassium *tert*-butoxide, DMF, 70 °C, 44%; (e) $N_2H_4{\bullet}H_2O$, methanol, reflux, 95 %; (f) 3,4,9,10-perylenetetracarboxylic dianhydride, $Zn(OAc)_2$, imidazole, 180 °C, 55%.

sented by **P1** and **P2** (Figure 1), that consist of alternating OPV and PERY segments connected via saturated spacers. The photophysics of these two alternating copolymers has been studied in detail both experimentally and theoretically. On one hand, fluorescence and femtosecond pump−probe spectroscopy in solution and in the solid state have been used to elucidate the temporal evolution of the photoexcited state and determine the rates for charge separation and recombination; the photophysical properties are compared to those of a cyclic model compound, **M1** (Figure 1), in which the two groups are held in a face-to-face orientation. On the other hand, correlated quantum-chemical calculations have been performed to determine the different molecular parameters that are involved in the charge separation and charge recombination rates in **P2** and **M1**; particular attention has been given to the role of the relative orientations of donor and acceptor chromophores on the electronic coupling and thermodynamic parameters for charge transfer. The photoinduced electron-transfer reactions in the polychromophoric alternating D−A arrays occur for **P1** and **P2** in the picosecond regime, both in solution and in the solid state. To explain the influence of the spacer length, we propose that there is a significant effect of the conformation of the polymer chain on the rate for photoinduced energy and electron transfer.

## Experimental Results and Discussion

**Synthesis.** The synthesis of polymers **P1** and **P2** and the cyclic model compound **M1** was accomplished using a palladium-catalyzed aryl−aryl coupling of appropriately functionalized perylene bisimide and oligo(*p*-phenylene vinylene) monomers **6**, **10**, and **13**. The synthesis of the perylene bisimide monomer **6** (Scheme 1) started with a convergent approach to the amine **5**. On one side, a Williamson etherification of 6-bromo-1-hexanol and 4-bromophenol afforded alcohol **1**, which was tosylated to give **2**. On the other side, the amine of (*S*)-(+)-leucinol was protected with a phthalimide group to imide **3**. A second Williamson etherification of alcohol **3** with tosylate **2** gave diether **4**, which was deprotected with hydrazine to the free amine **5**. Finally, reaction of 2 equiv of **5** with 3,4,9,10-perylenetetracarboxylic dianhydride (PTCDA) resulted in perylene bisimide **6**.

The second perylene bisimide monomer **10** was obtained following a slightly different strategy (Scheme 2). Reaction of (*S*)-(+)-leucinol with di-*tert*-butyl dicarbonate afforded BOC-protected amine **7**. A Mitsunobu reaction of **7** with 4-bromophenol was carried out to yield ether **8**. Deprotection of **8** by reaction with trifluoroacetic acid (TFA) and $NaHCO_3$ afforded amine **9**, which was reacted with PTCDA to perylene bisimide **10**.

The synthesis of the oligo(*p*-phenylene vinylene) (OPV) monomer **13** (Scheme 3) started with treatment of (*E*,*E*)-1,4-

(23) Nierengarten, J.-F.; Eckert, J.-F.; Nicoud, J.-F.; Ouali, L.; Krasnikov, V.; Hadziioannou, G. *Chem. Commun*. **1999**, 617.
(24) Eckert, J.-F.; Nicoud, J.-F.; Nierengarten, J.-F.; Liu, S.-G.; Echegoyen, L.; Barigelletti, F.; Armaroli, N.; Ouali, L.; Krasnikov, V.; Hadziioannou, G. *J. Am. Chem. Soc*. **2000**, *122*, 7467
(25) Peeters, E.; Van Hal, P. A.; Knol, J.; Brabec, C. J.; Sariciftci, N. S.; Hummelen, J. C.; Janssen, R. A. J. *J. Phys. Chem. B* **2000**, *104*, 10174.
(26) El-ghayoury, A.; Schenning, A. P. J. H.; Van Hal, P. A.; Van Duren, J. K. J.; Janssen, R. A. J.; Meijer, E. W. *Angew. Chem., Int. Ed.* **2001**, *40*, 3660−3663.
(27) Halls, J. J. M.; Friend, R. H. *Synth. Met.* **1997**, *85*, 1307.
(28) Schmidt-Mende, L.; Fechtenkotter, A.; Müllen, K.; Moons, E.; Friend, R. H.; MacKenzie, J. D. *Science* **2001**, *293*, 1119.
(29) Dittmer, J. J.; Marseglia, E. A.; Friend, R. H. *Adv. Mater*. **2000**, *12*, 1270.
(30) Dittmer, J. J.; Petritsch, K.; Marseglia, E. A.; Friend, R. H.; Rost, H.; Holmes, A. B. *Synth. Met*. **1999**, *102*, 879.
(31) Angadi, M. A.; Gosztola, D.; Wasielewski, M. R. *J. Appl. Phys*.**1998**, *83*, 6187.

***Scheme 2.*** Synthesis of the Perylene Bisimide Monomer **10**[a]

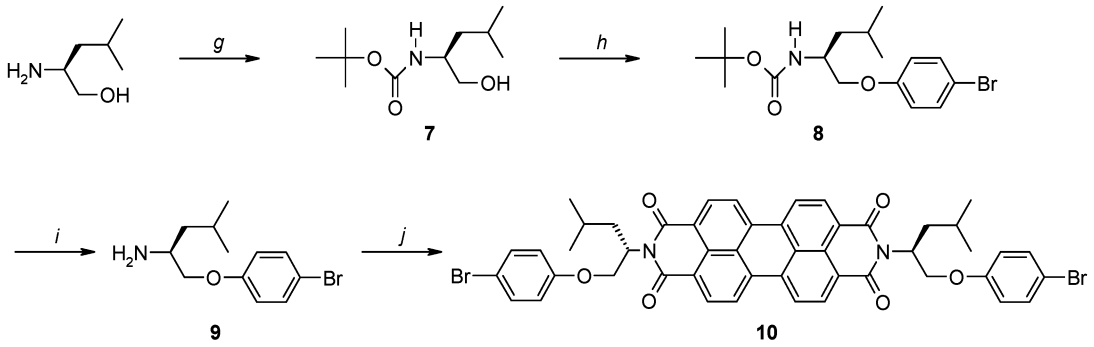

[a] (g) $BOC_2O$, THF, 97%; (h) 4-bromophenol, $PPh_3$, DEAD, toluene, 23%; (i) 1. TFA, $CH_2Cl_2$; 2. $NaHCO_3$, 76%; (j) 3,4,9,10-perylenetetracarboxylic dianhydride, $Zn(OAc)_2$, imidazole, 180 °C, 65%.

***Scheme 3.*** Synthesis of OPV Monomer **13**[a]

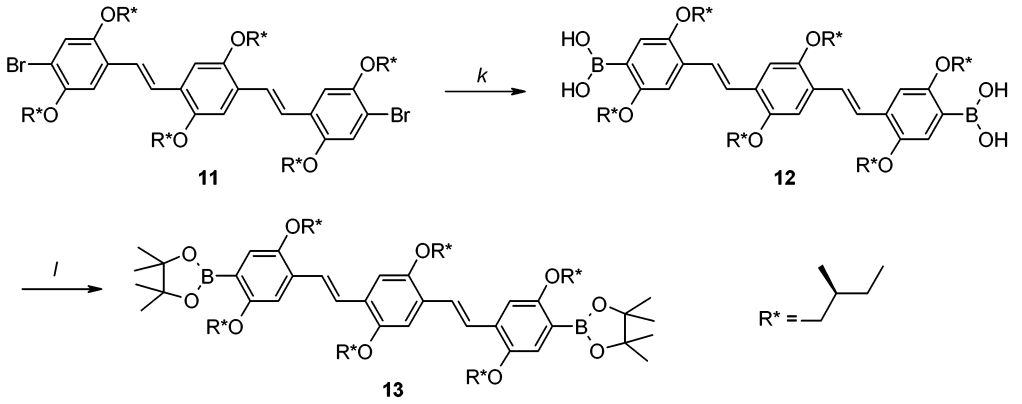

[a] (k) 1. n-BuLi, THF, −78 °C; 2. $B(OMe)_3$, −78 °C; 3. $H_2O$, 51%; (l) pinacol, $CH_2Cl_2$, reflux, 58%.

bis{4-bromo-2,5,-bis[(*S*)-2-methylbutoxy]styryl}-2,5-bis[(*S*)-2-methylbu toxy]benzene[11,32] with butyllithium and subsequent reaction with trimethyl borate and water to yield bisboronic acid **12**. Condensation of bisboronic acid **12** with pinacol resulted in the formation of the bisboralane **13**.

All monomers were fully characterized using $^1H$ and $^{13}C$ NMR spectroscopy, elemental analysis, and MALDI-TOF mass spectrometry.

Polymers **P1** and **P2** were synthesized by a Suzuki polymerization using $Pd(PPh_3)_4$ as a catalyst from equimolar amounts of bisboralane oligo(*p*-phenylene vinylene) monomer **13** and the perylene bisimide monomers **6** and **10,** respectively. Polymerization of **6** with **13** afforded, apart from **P1**, cyclic compound **M1** as a byproduct, which could be isolated and purified by extraction with acetone, column chromatography, and preparative size-exclusion chromatography (SEC).

Bis(4-methoxphenyl)-OPV3, **M2**, was synthesized by Suzuki coupling of **13** with 4-bromoanisol for comparison with the polymers in the optical experiments.

**Characterization of the Polymers.** The polymers were characterized by $^1H$ and $^{13}C$ NMR spectroscopy. In the $^1H$ NMR spectra of the polymers, the signals in the aromatic region have shifted compared to the spectra of the monomers. For **P1**, the signals of the protons of the bromophenyl ring at 7.14 and 6.46 ppm in monomer **6** shift to 7.47 and 6.81 ppm in the polymer. In the $^1H$ NMR of **P2** these signals appear at 7.48 and 6.91 ppm, compared to 7.29 and 6.76 ppm for monomer **10**. The $^1H$ NMR signals of the starting monomers could no longer be detected in the polymers. The molecular weight of the polymers determined by size-exclusion chromatography (SEC) versus polystyrene standards is $M_n$ = 12.6 kg/mol for **P1** and $M_n$ = 10.8 kg/mol for **P2** with polydispersities of 2.1 and 2.4, respectively. MALDI-TOF mass spectrometry on **P1** and **P2** was not successful but confirmed the cyclic structure of **M1** by reproducing the exact molar mass in a high-resolution spectrum.

**Absorption Spectra.** UV−vis absorption spectra of polymers **P1** and **P2** in toluene solution are shown in Figure 2, together with the absorption spectra of the model compounds **M2** and **M3**.[33] Absorption bands of the PERY chromophore appear at 460, 490, and 525 nm, while the OPV absorption peaks at ∼425 nm. As can be seen in Figure 2, the spectra of the two polymers are almost identical and close to a linear superposition of the spectra of **M2** and **M3**. This demonstrates that in the two polymers the two chromophores are indeed present in a 1:1 ratio.

The absorption spectra of **P1** and **P2** give no indication of a major electronic interaction between the OPV and PERY chromophores in the ground state. The absorption spectra further reveal that the singlet excited state of the PERY unit lies below that of the OPV chromophore. As a result, excitation of the OPV chromophore may result in singlet energy transfer to the PERY unit. Such excitation transfer has recently been described in perylene-end-capped polyindenofluorene.[34,35]

For **M1** such an electronic interaction is much more likely because the two chromophores are in close proximity. Moreover, the enantiomerically pure (*S*)-2-methylbutoxy side chains of the

(32) Jonkheijm, P.; Fransen, M.; Schenning, A. P. H. J.; Meijer, E. W. *J. Chem. Soc., Perkin Trans. 2* **2000**, 1280.

(33) Demmig, S.; Langhals, H. *Chem. Ber*. **1988**, *121*, 225.

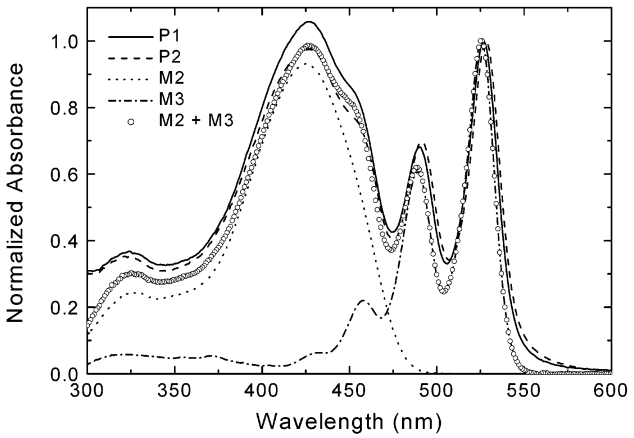


***Figure 2.*** Absorption spectra of polymers **P1** and **P2** and compounds **M2** and **M3** dissolved in toluene. The spectra of **P1**, **P2**, and **M3** have been normalized at 527 nm. The spectrum of **M2** is normalized with respect to that of **M**3 to represent similar concentrations. The open circles represent the spectrum of a 1:1 molar mixture of **M2** and **M3**.

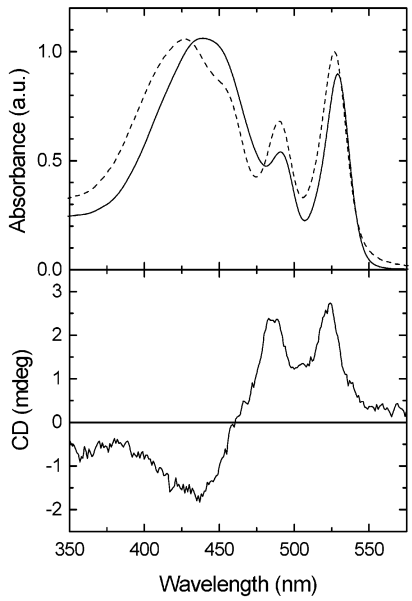


***Figure 3.*** Absorption (top) and circular dichroism (bottom) spectra of compound **M1** (solid lines) in toluene. For comparison the absorption spectrum of **P1** is shown (dashed line).

OPV fragment and the two (*S*) stereocenters of the leucinol group could give rise to preferential helical twisting of the OPV and PERY chromophores in the face-to-face orientation present in **M1**. The UV−vis absorption spectrum of **M1** (Figure 3) shows that, compared to **P1**, there is a small but distinct red shift of the OPV band from 428 to 439 nm. The circular dichroism (CD) spectrum of **M1** (Figure 3) reveals a Cotton effect, with a negative part at 438 nm (OPV) and a positive part at 486 and 524 nm (PERY). Following the exciton-coupling model,[36] a bisignated Cotton effect is consistent with two interacting chromophores in a helical orientation. Exciton theory of chiral bichromophoric systems suggests that the positive Cotton effect of **M1** at the higher wavelengths indicates that transition dipole moments of the OPV and PERY chromophores in **M1** are in a right-handed twisted conformation.[36] From these results **M1** emerges as a new chiral macrocycle consisting of two electronically different interacting conjugated chromophores. Chiral macrocycles with two identical chromophores have been described recently.[37,38]

**Electrochemistry.** The oxidation and reduction potentials of the oligo(*p*-phenylene vinylene) and perylene bisimide segments were determined by cyclic voltammetry in dichloromethane (vs SCE). Two reversible oxidation waves were found for **M2** at half-wave potentials of $E_{ox,1} = 0.80$ V and $E_{ox,2} = 0.94$ V. For **M3** the reduction potentials were determined at $E_{red,1} = -0.65$ V and $E_{red,2} = -0.85$ V.

**Energy for Charge Separation.** The redox potentials can be used to estimate the Gibbs free energy of the intramolecular charge-separated state ($G_{cs}$) of the donor−acceptor polymers **P1** and **P2** and of the cyclic dyad **M1** with respect to the electronic ground state in a solvent with polarity $\epsilon_s$ via the Weller equation[39]

$$G_{cs} = e(E_{ox}(D) - E_{red}(A)) - \frac{e^2}{4\pi\epsilon_0\epsilon_s R_{cc}} - \frac{e^2}{8\pi\epsilon_0}\left(\frac{1}{r^+} + \frac{1}{r^-}\right)\left(\frac{1}{\epsilon_{ref}} - \frac{1}{\epsilon_s}\right) \quad (1)$$

To calculate $G_{CS}$, the oxidation potential of the donor $E_{ox}(D)$ and the reduction potential of the acceptor $E_{red}(A)$ of **M2** and **M3**, determined in dichloromethane ($\epsilon_{ref} = 8.93$), were used. The radius of the PERY anion ($r^- = 4.71$ Å) was estimated from the density ($\rho = 1.59$ g cm$^{-3}$) of *N,N'*-dimethylperylene-3,4:9,10-tetracarboxylic-bisimide from the X-ray crystallographic data via $r^- = [3M/(4\pi\rho N_A)]^{1/3}$.[40] The radius of the positive ion of OPV segment was estimated to be $r^+ = 5.05$ Å.[25] The distance between the centers of donor and acceptor moieties, $R_{cc}$, was determined from geometries of **M1**, **P1**, and **P2** optimized at the molecular mechanics level with the Dreiding and Universal force fields; these values are 4, 31, and 22 Å for **M1**, **P1**, and **P2**, respectively. Because **P1** has a flexible spacer between the OPV and PERY moieties, the distance of 31 Å for **P1** is an upper limit corresponding to the fully extended structure. We assume that the value of 4 Å is the lower limit for $R_{cc}$ in **P1** in analogy with the situation in **M1**. With these parameters we find that the intramolecular charge-separated state in **M1**, **P1**, and **P2** lies at lower energy than those of the OPV or PERY singlet excited states (Table 1, Figure 4) in toluene ($\epsilon_s = 2.38$). Hence, photoinduced electron transfer is expected to be an exergonic reaction for these systems.

**Fluorescence Spectra and Fluorescence Quenching.** To investigate the photophysics and especially address the possibility of photoinduced energy or electron-transfer reactions between the donor and acceptor moieties of the polymers **P1** and **P2**, their fluorescence was studied in toluene solution. The fluorescence spectra of **M2** and of the two polymers recorded with (preferential) excitation of the OPV chromophore at 410 nm reveal that in **P1** and **P2** the OPV fluorescence at 482 nm is quenched (Figure 5). Compared to **M2**, the OPV fluorescence

(34) Herz, L. M.; Silva, C.; Friend, R. H.; Phillips, R. T.; Setayesh, S.; Becker, S.; Marsitsky, D.; Müllen, K. *Phys. Rev. B* **2001**, *64*, 195203.
(35) Beljonne, D.; Pourtois, G.; Silva, C.; Hennebicq, E.; Herz, L. M.; Friend, R. H.; Scholes, G. D.; Setayesh, S.; Mullen, K.; Brédas, J. L. *Proc. Natl. Acad. Sci.* **2002**, *99*, 10982.
(36) Harada, N.; Nakanishi, K. *Circular Dichroic Spectroscopy. Exciton Coupling in Organic Stereochemistry*; University Science Books, Mill Valley, CA, 1983.
(37) Köhler, B.; Enkelmann, V.; Oda, M.; Pieraccini, S.; Spada, G. P.; Scherf, U. *Chem. Eur. J.* **2001**, *7*, 3000.
(38) Langhals, H.; Ismael, R. *Eur. J. Org. Chem.* **1998**, *1915*, 5.
(39) Weller, A. Z. *Phys. Chem. Neue Folge* **1982**, *133*, 93.
(40) Hädicke, E.; Graser, F. *Acta Crystallogr., Sect. C* **1986**, *42*, 189.

***Table 1.*** Free Energy of Intramolecular and Intermolecular Charge-Separated States Calculated from Eq 1 in Toluene and Relative to the Ground State and the Singlet Excited States of OPV and PERY[a]

| | | | $\Delta G_{CS} = G_{CS} - E_{00}$ (eV) | |
|---|---|---|---|---|
| | $R_{CC}$ (Å) | $G_{CS}$ (eV) | $S_1$ OPV | $S_1$ PERY |
| **M1** | 4 | 0.85 | −1.74 | −1.46 |
| **P1** | 31[b] | 2.17 | −0.42 | −0.15 |
| **P2** | 22[b] | 2.09 | −0.50 | −0.23 |
| **M2 + M3** | ∞ | 2.36 | −0.23 | 0.05 |

[a] The following parameters were used: $E_{ox}(D) = 0.80$ V, $E_{red}(A) = -0.65$ V, $r^+ = 5.05$ Å, $r^- = 4.70$ Å, $\epsilon_s = 2.38$, $\epsilon_{ref} = 8.93$. For OPV($S_1$): $E_{00} = 2.59$ eV. For PERY($S_1$): $E_{00} = 2.31$ eV. [b] Assuming a fully extended structure of the spacer.

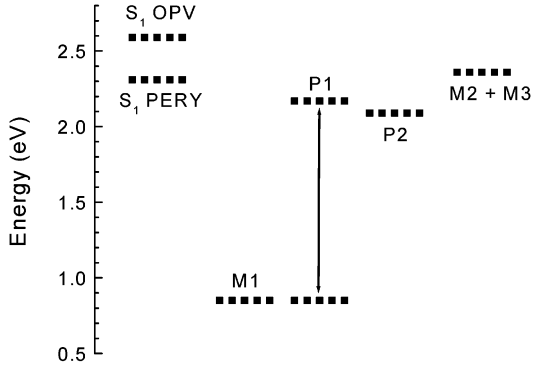


***Figure 4.*** Energies of the singlet excited states of the OPV and PERY chromophores; the intramolecular charge-separated states of **M1**, **P1,** and **P2** and the intermolecular charge-separated state between **M2** and **M3**. The energy levels of the charge-separated states were calculated from eq 1 using the parameters described in the text and assuming toluene ($\epsilon_s = 2.38$) as the solvent. The range of values for **P1**, depending on $R_{cc}$, is given by the arrow.

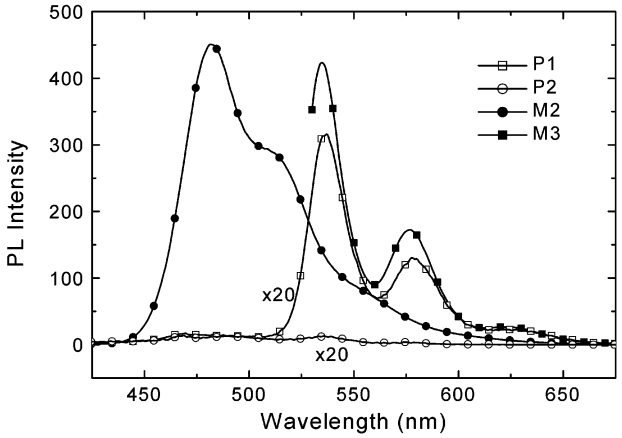


***Figure 5.*** Fluorescence emission spectra of polymers **P1** and **P2** and OPV-model **M2** upon (preferential) excitation of the OPV chromophore at 410 nm and of PERY-model **M3** upon excitation at 525 nm. The spectra are corrected for the optical density at the excitation wavelength. The spectra of the polymers are multiplied by 20 for clarity.

is reduced by a factor of $Q = 650$ for **P1** and $Q = 700$ for **P2** (Table 2). Comparison with the fluorescence spectrum of perylene bisimide model **M3**, recorded with excitation at 525 nm, shows that both polymers give some emission that originates from the PERY chromophore. When the perylene bisimide segments of **P1** and **P2** were selectively excited at 525 nm, it became evident, however, that also the PERY emission in the polymers is strongly quenched. Quenching factors of 30 and 630 (Table 2) were found for the perylene emission of **P1** and **P2**, respectively, relative to that of **M3**. For the cyclic model compound **M1**, photoluminescence of the OPV chromophore could no longer be identified ($Q > 15000$), indicating a very efficient deactivation of its singlet excited state. The quenching of the PERY emission in **M1** was substantial ($Q = 270$, Table 2) but less than that for **P2**.

These results can be rationalized by considering the diagram shown in Figure 6. After photoexcitation of the OPV chromophore, the intrinsic radiative ($k_r$) and nonradiative decay ($k_{nr}$) of the donor can be quenched by either a singlet energy transfer reaction ($k_{et}$) to the PERY chromophore or a charge separation ($k_{cs}$) to a charge-separated state (CSS) in which an electron is transferred from the OPV to the PERY unit. Photoexcitation of the PERY unit, however, cannot give singlet energy transfer because it is endergonic, but charge separation can still occur, resulting in quenching of the PERY fluorescence.

From the quenching of the PERY emission in **P1**, **P2**, and **M1** we conclude that in these systems electron transfer takes place when the acceptor unit is photoexcited. To examine whether singlet energy transfer occurs, the excitation spectra of the PERY emission at 579 nm were recorded in toluene.[41] Figure 7 shows that in the excitation spectrum of the PERY emission of **P1** and **P2** both chromophores contribute to an equal extent. This indicates that the rate for singlet energy transfer from the OPV singlet state ($k_{et}$, Figure 6) in **P1** and **P2** is at least of the same order of magnitude as the rate for direct electron transfer ($k_{cs}^d$, Figure 6). In contrast, the excitation spectrum of **M1** differs from its absorption spectrum in the 400−475 nm region (Figure 7). This suggests that direct electron transfer from the $S_1$ state of OPV is more important here.

**Photoinduced Absorption in Thin Films.** To investigate the photoinduced electron-transfer processes in more detail, we performed photoinduced absorption (PIA) spectroscopy on long and short time scales.

The near steady-state PIA spectrum of a thin film of **P1** on quartz, recorded with excitation at 528 nm at 80 K (Figure 8), shows the formation of $PERY^{-\bullet}$ radical anions and $OPV^{+\bullet}$ radical cations. The peaks at 1.28, 1.54, and 1.72 eV are readily attributed to the $PERY^{-\bullet}$ radical anion bands.[42] The absorption band at 0.72 eV is assigned to the $OPV^{+\bullet}$ radical cations; its position is between the absorption bands of $OPV3^{+\bullet}$ and $OPV4^{+\bullet}$ radical cations.[43] Comparison with spectra of $OPV3^{+\bullet}$ and $OPV4^{+\bullet}$ indicates that a second absorption of the $OPV^{+\bullet}$ radical cation in **P1** is expected to overlap with the $PERY^{-\bullet}$ radical anion bands in the 1.5−2.0 eV region. An almost identical PIA spectrum was recorded for polymer **P2** (Figure 8). Moreover, the PIA spectrum does not depend on whether the sample is irradiated at 458 nm (preferential excitation of OPV) or at 528 nm (selective excitation of PERY). This demonstrates that both hole and electron-transfer processes take place in the solid state.

The PIA signals of both **P1** and **P2** were found to increase in a nonlinear fashion with the intensity of the excitation beam following a power-law behavior with an exponent on the order of 0.6−0.7, indicating that bimolecular decay processes, such as nongeminate charge recombination, contribute to the decay.

(41) It is important to note that small concentrations of fluorescent impurities, such as monomers, can mask the true excitation spectra of these weakly fluorescent systems, and the data should be interpreted with caution.
(42) Salbeck, J. *J. Electroanal. Chem.* **1992**, *340*, 169−195.
(43) Van Hal, P. A.; Beckers, E. H. A.; Peeters, E.; Apperloo, J. J.; Janssen, R. A. J. *Chem. Phys. Lett.* **2000**, *328*, 403−408.

***Table 2.*** Rate Constants for Energy Transfer, Direct and Indirect Charge Separation, and Charge Recombination As Obtained from Photoluminescence Quenching and Pump−Probe PIA Spectroscopy for **P1**, **P2**, and **M1** in Toluene Solution and Solid Films

| | | PL quenching | | | | PIA OPV[a] | | PIA PERY[b] | |
|---|---|---|---|---|---|---|---|---|---|
| | | $Q_{OPV}$[c] | $Q_{PERY}$[c] | $(k_{et} + k_{cs}^{d})$[d] ($ns^{-1}$) | $k_{cs}^{i}$[e] ($ns^{-1}$) | $k_{cs}^{d}$ ($ns^{-1}$) | $k_{rec}$ ($ns^{-1}$) | $k_{cs}^{i}$ ($ns^{-1}$) | $k_{rec}$ ($ns^{-1}$) |
| **P1** | toluene | 650 | 30 | 540 | 7 | 630 | 1.9 | 1400 | 1.4 |
| | film | | | | | ≥2300 | 9.5 | | |
| **P2** | toluene | 700 | 630 | 580 | 160 | 350 | 0.6 | 270 | 0.5 |
| | film | | | | | ≥2300 | 9.5 | | |
| **M1** | toluene | ≥15000 | 270 | ≥12500 | 70 | 1700 | 6.9 | 1200 | 5.9 |

[a] Excitation of the OPV chormophore at 450 nm. [b] Excitation of the PERY chromophore at 520 nm. [c] Excitation of OPV at 410 nm and PERY at 525 nm. [d] From $Q_{OPV}$ and eq 2. [e] From $Q_{PERY}$ and eq 3.

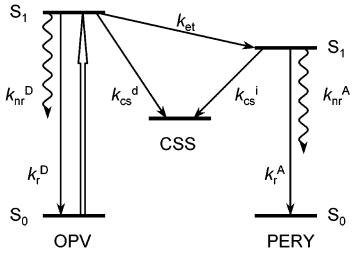


***Figure 6.*** Jablonski diagram representing the different photophysical events that can take place in the donor−acceptor (D−A) polymers **P1** and **P2** and model **M1** upon excitation of the OPV chromophore (open arrow). The singlet energy transfer ($k_{et}$), the direct ($k_{cs}^{d}$) and indirect ($k_{cs}^{i}$) electron transfer, the radiative emission ($k_r$), and nonradiative emission ($k_{nr}$) are indicated.

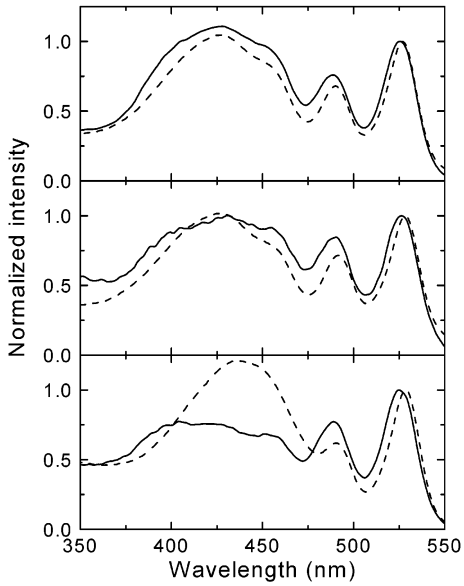


***Figure 7.*** Normalized absorption (dashed lines) and excitation (solid lines) spectra of polymer **P1** (top), polymer **P2** (middle), and model **M1** recorded in toluene ($\lambda_{em} = 579$ nm).

All PIA bands exhibited an almost identical dependence on changing the modulation frequency, which could be fitted to a combined expression of a power-law dependence and bimolecular decay,[44] giving exponents from −0.40 to −0.45 and lifetimes in the range from 1 to 2 ms.

Films of **P1** and **P2** were also investigated with femtosecond pump−probe spectroscopy. In Figure 9 the normalized change in transmission $\Delta T/T$ at 1450 nm (0.86 eV) for both polymers is plotted versus the time delay after excitation with a ∼150 fs pulse at 450 nm. At this probe wavelength a negative differential

(44) Van Hal, P. A.; Christiaans, M. P. T.; Wienk, M. M.; Kroon, J. M.; Janssen, R. A. J. *J. Phys. Chem. B* **1999**, *103*, 4352.

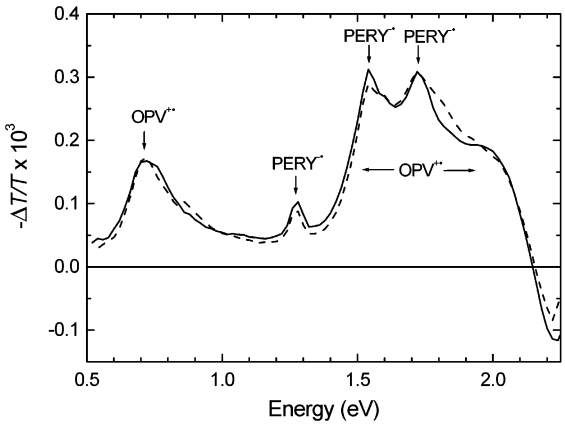


***Figure 8.*** Near steady-state photoinduced absorption spectra of **P1** (solid line) and **P2** (dashed line) as thin films on quartz recorded at 80 K. Excitation wavelength is 528 nm, modulation frequency 275 Hz.

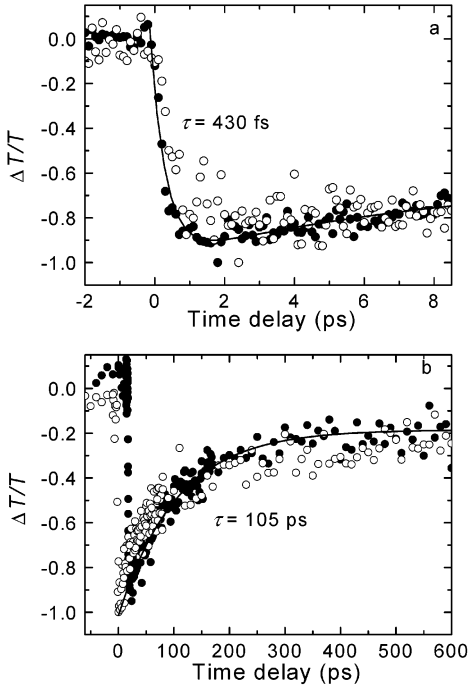


***Figure 9.*** Normalized differential transmission dynamics of films of polymers **P1** (●) and **P2** (○) at room temperature, recorded at 1450 nm (low-energy absorption of OPV radical cations) after excitation at 450 nm. Solid lines are fits to exponential growth (a) and decay (b).

transmission is observed, consistent with the fact that at 1450 nm we exclusively probe the formation of $OPV^{+\bullet}$ radical cations and hence the event of photoinduced charge separation. Figure 9 shows that the rate for charge separation (∼0.4 ps) is extremely fast for both **P1** and **P2** in the film. The recombination process

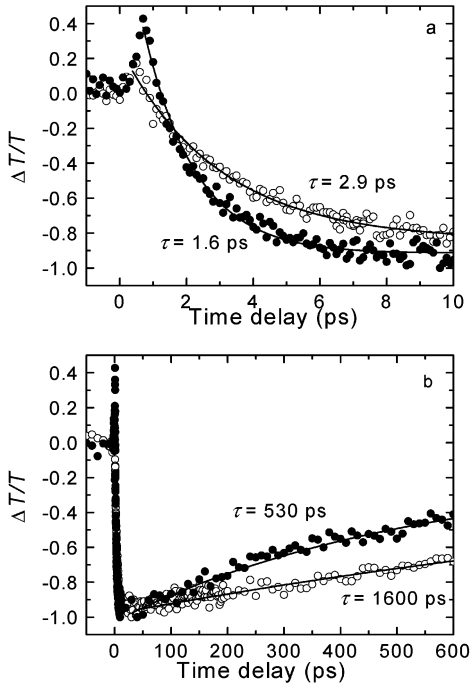


***Figure 10.*** Normalized differential transmission dynamics of polymers **P1** (●) and **P2** (○) in toluene solution at room temperature, recorded at 1450 nm (low-energy absorption of OPV radical cations) after excitation at 450 nm. Solid lines are fits to monoexponential growth (a) and decay (b).

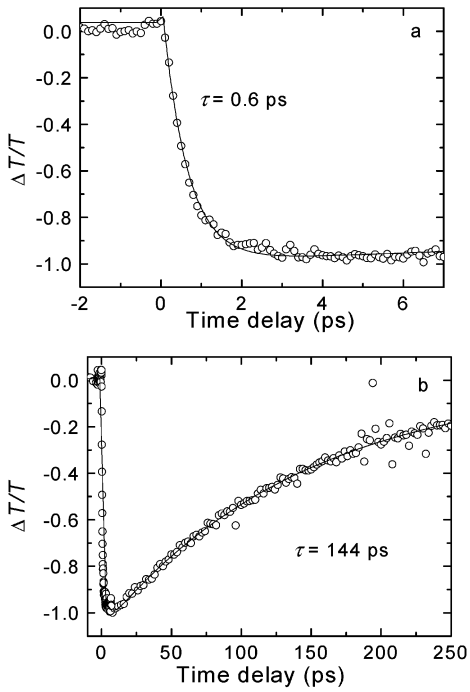


***Figure 11.*** Normalized differential transmission dynamics of **M1** in toluene solution at room temperature, recorded at 1450 nm (low-energy absorption of OPV radical cations) after excitation at 450 nm. Solid lines are fits to monoexponential growth (a) and decay (b).

contains several components. At short times after photoexcitation the recombination is dominated by a process occurring with a time constant of ∼105 ps; however, after 600 ps, ca. 20% of the charge is still present in both polymer films. These residual charges decay very slowly. We interpret the 105 ps decay as geminate recombination and attributed the longer lived components to those charges that diffuse away from their original position and eventually may become trapped.

**Photoinduced Absorption in Solution.** Femtosecond pump−probe spectroscopy was also used to study polymers **P1** and **P2** in toluene solution (Figure 10). Again, the OPV chromophore was excited at 450 nm and the change in transmission of the $OPV^{+\bullet}$ radical cation band at 1450 nm was probed in time. While in the solid state **P1** and **P2** behave very similarly, significant differences are observed in solution. In toluene, charge separation in **P1** (∼1.6 ps) is faster than that in polymer **P2** (∼2.9 ps). Both are somewhat slower than that in the solid state. Also, the rate for charge recombination in solution is lower than in the films. Fitting a monoexponential decay to the data for **P1** and **P2** (Figure 10) provides time constants for recombination of positive and negative charges of 530 and 1600 ps, respectively. As a result of the difference in rate constants, ∼75% of the charges are still present after 600 ps in **P2** and ∼40% in **P1**. The rates of charge separation and charge recombination are summarized in Table 2.

Pump−probe experiments have also been performed with excitation at 520 nm, where the PERY chromophore is directly excited again with probing at 1450 nm to observe $OPV^{+\bullet}$ radical cations. The results (Table 2) are similar to those obtained with excitation at 450 nm and demonstrate that $k_{cs}^{d}$ and $k_{cs}^{i}$ are of the same order of magnitude.

Transient pump−probe experiments on **M1** in toluene solution (Figure 11) have been performed for comparison to the data of **P1** and **P2** in solution and film. The forward charge transfer upon photoexcitation of **M1** in toluene is significantly faster than that for **P1** and **P2** in the same solvent. Actually, the time constant of ∼0.6 ps for the forward reaction is close to that observed in films of **P1** and **P2**. The back electron transfer (recombination) in **M1** is monoexponential with a time constant of ∼144 ps. The recombination rate of **M1** is therefore higher than that of **P1** and **P2** in solution but close to values observed in the polymer films. Similar to **P1** and **P2**, photoexcitation of the PERY chromophore at 520 nm instead of OPV provided comparable values for the rate for charge separation. The close correspondence in charge formation and recombination between **M1** in toluene and the **P1** and **P2** films can be rationalized by considering that the face-to-face orientation of the OPV and PERY photoactive groups in **M1** is also present in the solid-state films of **P1** and **P2**.

**Photovoltaic Devices.** Photovoltaic devices were prepared by spin casting solutions of **P1** and **P2** in chloroform on indium tin oxide covered with a layer of polyethylenedioxythiophene polystyrenesulfonate (PEDOT:PSS, Bayer AG) as the transparent front electrode. A LiF/Al back electrode was deposited in a vacuum. The *I-V* characteristics of the ITO/PEDOT:PSS/polymer/LiF/Al devices were measured in the dark and under simulated AM1.5 conditions (Figure 12). Both polymers gave similar results. Although the open-circuit voltage in both cells is relatively high ($V_{OC}$ = 1.20 and 0.97 V, for **P1** and **P2**, respectively), the short-circuit current density ($J_{SC}$ = 0.008 mA $cm^{-2}$ for **P1** and $J_{SC}$ = 0.012 mA $cm^{-2}$ for **P2**) and the fill factor (FF = 0.25−0.26) are low. The low currents are attributed to poor transport characteristics, because the initial charge generation is efficient as inferred from fluorescence quenching in the films.

**Kinetics of Electron and Energy Transfers.** Fluorescence quenching and pump−probe experiments can be used to estimate the rate constants for energy transfer ($k_{et}$) and for direct and

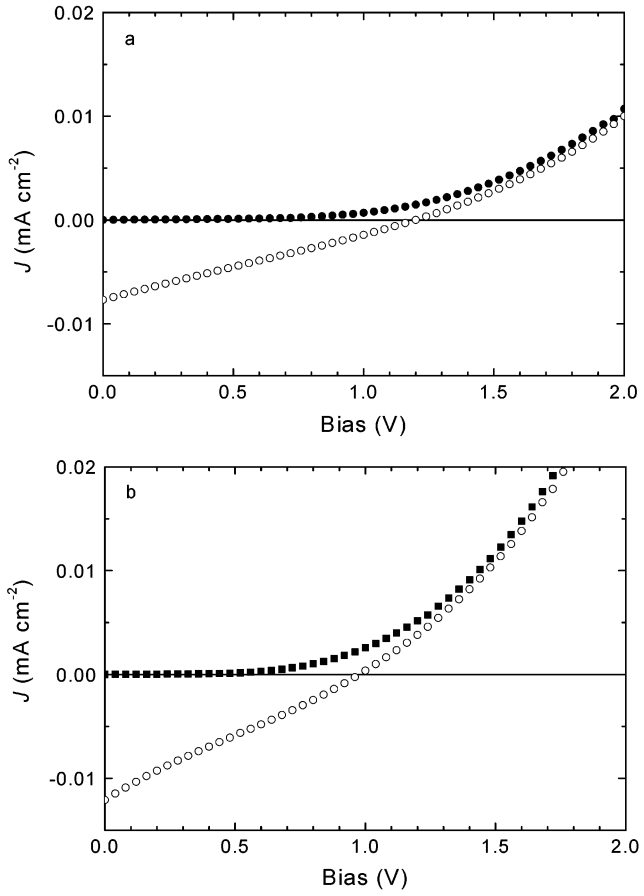


***Figure 12.*** Current density−voltage characteristics of photovoltaic devices (ITO/PEDOT:PSS/polymer/LiF/Al) of polymers **P1** (a) and **P2** (b) in the dark (●) and under simulated AM1.5 illumination (100 mW/cm$^2$) (○).

indirect charge separation ($k_{cs}^{d}$ and $k_{cs}^{i}$, respectively) (Figure 6). The sum of $k_{et}$ and $k_{cs}^{d}$ can be related to the quenching of the OPV fluorescence ($Q_{OPV}$) using the fluorescence lifetime of the donor segment ($\tau_{OPV}$) via

$$k_{et} + k_{cs}^{d} = \frac{Q_{OPV} - 1}{\tau_{OPV}} \qquad (2)$$

In a similar fashion it is possible to relate the quenching of the PERY fluorescence to the rate for the indirect charge separation

$$k_{cs}^{i} = \frac{Q_{PERY} - 1}{\tau_{PERY}} \qquad (3)$$

The fluorescence lifetimes of **M2** and **M3** in toluene solution were determined by time-correlated single-photon counting. The time-resolved fluorescence signal followed a monoexponential decay with time constants of 1.2 and 4.0 ns for **M2** and **M3**, respectively. The use of eqs 2 and 3 is not without difficulty because small concentrations of fluorescent impurities, such as monomers, can easily lead to an underestimation of the actual quenching. Pump−probe experiments generally give more reliable numbers because they probe the bulk of the sample.

The results are collected in Table 2. The OPV fluorescence quenching in **P1** and **P2** in toluene indicates that in the polymers $k_{et} + k_{cs}^{d} = 5.4-5.8 \times 10^{11}$ s$^{-1}$; while the rate is much higher in the cyclic molecule **M1** ($k_{et} + k_{cs}^{d} \geq 1.2 \times 10^{13}$ s$^{-1}$). The data are in satisfactory agreement with the rates for direct charge

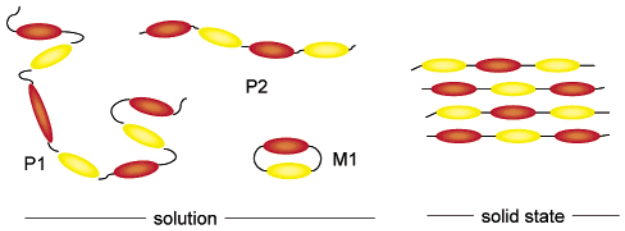


***Figure 13.*** Cartoon representation of the conformation of alternating donor−acceptor copolymers in solution. Donor (red) and acceptor (yellow) units are linked by long (**P1**) or short (**P2**) spacers. Face-to-face contacts of the two chromophores in **P1** enhance the rates for photoinduced energy and electron transfer compared to the end-to-end orientation in **P2**. In the solid-state face-to-face interactions, like the one enforced in **M1**, are omnipresent for both **P1** and **P2** via interchain interactions.

formation derived from pump−probe spectroscopy: $k_{cs}^{d} = 6.3 \times 10^{11}$ s$^{-1}$ for **P1**, $3.5 \times 10^{11}$ s$^{-1}$ for **P2**, and $\geq 1.7 \times 10^{12}$ s$^{-1}$ for **M1** (Table 2). The significantly lower value for **M1** in the latter experiment is limited by the time resolution of the pump−probe spectroscopy (0.4−0.5 ps), and hence, the value obtained from the OPV quenching is probably more accurate here. Although these results cannot be used to unravel the individual contributions of $k_{et}$ and $k_{cs}^{d}$ in a reliable fashion, the fluorescence excitation experiments have shown that these processes are competitive.

Comparison of the pump−probe PIA data shows that the rate for direct charge separation in toluene solution decreases in the sequence **M1**, **P1**, and **P2** (Table 2). The high rate for **M1** is consistent with a face-to-face orientation of the two chromophores, which ensures an efficient electronic coupling in the excited state, vide infra. The higher rate for **P1** than **P2** is at first sight surprising because of the longer spacer between the OPV and PERY groups in **P1**. This difference may be rationalized by the fact that the conformation of **P1** is heterogeneous on the picosecond time scale. The origin of this heterogeneity is the conformational flexibility of the polymer chain, which implies that the OPV and PERY segments can be in a range of conformations from fully extended (∼31 Å) to face-to-face (∼4 Å). The face-to-face orientation, which likely results in a high rate ($k_{cs}^{d}$), is not possible for **P2** because the spacer is more rigid. These differences are schematically shown in Figure 13. The rate for charge recombination ($k_{rec}$) decreases in the sequence **M1**, **P1**, **P2** and, hence, follows the same trend as that observed for charge separation. It is likely that similar conformational differences are the cause for this result. At present it is unknown whether migration of photogenerated charges along the polymer chain occurs. The most likely mechanism for such a process would certainly involve folding to circumvent that positive (or negative) charges must reside on or hop over acceptor (or donor) units.

The rates for indirect charge separation, i.e., originating from the excited state of the PERY acceptor, in **M1**, **P1**, and **P2** as determined by pump−probe spectroscopy are similar to those for direct charge transfer (Table 2). As can be seen in Table 2, the values obtained from pump−probe spectroscopy differ significantly from those determined from the PERY fluorescence quenching, especially for **P1** and **M1**. The presence of a small (less than 0.4%) impurity containing the PERY chromophore can explain this discrepancy for **M1**, but for **P1** we consider that the rather low PL quenching ($Q_{PERY} = 30$) is, at least in part, intrinsic. In a fully extended conformation of the linker

(~31 Å) of **P1** the electronic coupling of the OPV and PERY chromophores is negligible in the excited state and, hence, a low rate for electron transfer, causing a decreased quenching of the PERY emission. Because singlet energy transfer is less dependent on the distance than electron transfer, the OPV fluorescence in **P1** is quenched to the same extent as in **P2**. The conformational freedom of **P1** can thus be used to rationalize the widely different values obtained for $k_{cs}^{i}$ using PL quenching and PIA spectroscopy.

The rate for charge separation in the films of **P1** and **P2**, $k_{cs}^{d} \geq 2.3 \times 10^{12}$ s$^{-1}$, is at the limit of the time resolution of the pump−probe setup. The recombination, $k_{rec} = 9.5 \times 10^{9}$ s$^{-1}$, is much slower. Both processes, however, are significantly faster than the corresponding reactions in toluene solution. The increased rate for charge separation can be understood by assuming that in the films face-to-face orientations of the OPV and PERY chromophores (like the one in **M1**) are present (Figure 13). Although we have no evidence from morphological studies, several polymer materials[45−48] exist in which electron-rich (donor) and electron-deficient (acceptor) segments form alternating stacks in solution and in the solid state. The driving force for such orientations is the $\pi$-stacking in combination with electrostatic or weak charge-transfer interaction.[49,50] Also, in D−A molecular crystals the usual case is to have stacks with alternating D−A molecules.[51] A preference for face-to-face D−A interactions, as schematically drawn in Figure 13, contrast with the microphase separation that often occurs in block copolymers. Apparently, the tendency for the OPV and PERY segments to give alternating stacks in thin films of **P1** and **P2** is stronger than the antagonistic interactions that direct the microscopic phase separation. One likely explanation for this result is the limited length of the D and A segments in **P1** and **P2**. The proposition of the presence of alternating stacks of OPV and PERY in films of **P1** and **P2** is supported by the similar values of $k_{cs}^{d}$ obtained for **M1** and the polymer films (Table 2). In full agreement with this view, the initial recombination in the films is fast and the rate constant ($k_{rec} = 9.5 \times 10^{9}$ s$^{-1}$) is again similar to the one observed for **M1** ($k_{rec} = 6.9 \times 10^{9}$ s$^{-1}$). The long-lived charge carriers in the films result from those charges that escape from geminate recombination and diffuse to different sites in the films. The relatively low number of charges (<20%, Figure 9) that live up to 1 ns explains, at least in part, the low currents observed in photovoltaic cells made from **P1** and **P2**. If the face-to-face orientations of OPV and PERY are predominant in the films, this could be a more important reason for the low currents, because such orientation would severely limit charge transport.

**Theoretical Modeling of Charge Separation and Recombination.** Correlated semiempirical quantum-chemical calculations have been performed on the model compound **M1** and a monomer unit of **P2** to assess the various molecular parameters relevant in the charge separation and recombination processes. For the former process we have considered the cases where the charge transfer is induced by excitation of either the OPV donor (D*A → D$^+$A$^-$ process; that is the direct transfer, corresponding to electron transfer from D to A) or the acceptor (DA* → D$^+$A$^-$ process; that is the indirect transfer, corresponding to hole transfer from A to D).

The ground-state geometries of the full chemical structures have been optimized by means of the AM1 (Austin Model 1) method.[52] In the case of **M1**, the intermolecular geometric parameters were optimized at the molecular mechanics level using the Dreiding force field. To build the excited-state and charge-separated geometrical structures, the equilibrium geometries of the isolated donor and acceptor chromophores were first optimized in the lowest singlet excited state and in the singly (positively and negatively) charged ground state at the AM1/CAS-CI (complete active space-configuration interaction)[53] and AM1/ROHF (restricted open-shell Hartree−Fock) level, respectively; these were then combined into the whole structure to yield the relaxed geometries of the D*A, DA*, and D$^+$A$^-$ electronic states.

The transfer rate $k_{CS}$ and $k_{CR}$, corresponding to the probability for charge separation (D*A or DA* → D$^+$A$^-$) and charge recombination (D$^+$A$^-$ → DA) to occur after photoexcitation, respectively, are evaluated using Jortner's expression.[54,55] Going from reactant R to product P, the expression writes

$$k_{RP} = \frac{2\pi}{\hbar} V_{RP}^{2} \left(\frac{1}{4\pi\lambda_s kT}\right)^{1/2} \sum_{v} e^{-S} \frac{S^v}{v!} \times \exp\left(-\frac{(\Delta G^\circ + \lambda_s + v\hbar\langle\omega\rangle)^2}{4\lambda_s kT}\right) \quad (4)$$

Here, $V_{RP}$ is the electronic coupling representing the tunneling probability between the reactant and product potential-energy surfaces (approximated as harmonics), $\Delta G^\circ$ is the variation in Gibbs free energy during the reaction, $S$ (= $\{\lambda_i\}/\{\hbar\langle\omega_i\rangle\}$) is the Huang−Rhys factor expressed in terms of the intramolecular reorganization energy $\lambda_i$ and the effective mode vibrational energy $\hbar\langle\omega_i\rangle$, and $\lambda_s$ is the solvent reorganization energy including contributions from the polarization changes in the dielectric (solvent) environment.

$\Delta G^\circ$ is estimated from the enthalpies of formation, $\Delta H_f^\circ$, with the solvent taken into account through the use of the COSMO model[56] implemented in the AMPAC package:[57]

$$\Delta G^\circ = \Delta H_P^\circ - \Delta H_R^\circ + E_{cb}$$

with

$$E_{cb} = \frac{1}{4\pi\epsilon_0} \sum_{i}^{D} \sum_{j}^{A} \frac{q_i q_j}{\epsilon_s r_{ij}}$$

$$\Delta H_P^\circ = \Delta H_{f,D^+}^\circ + \Delta H_{f,A^-}^\circ; \quad (5)$$

$$\Delta H_R^\circ = \Delta H_{f,D^*}^\circ + \Delta H_{f,A}^\circ \text{ or } \Delta H_{f,D}^\circ + \Delta H_{f,A^*}^\circ$$

$\epsilon_0$ and $\epsilon_s$ are the vacuum and solvent dielectric constants,

(45) Lokey, S. R.; Iverson, B. L. *Nature* **1995**, *375*, 303.
(46) Zych, A. J.; Iverson, B. L. *J. Am. Chem. Soc.* **2000**, *122*, 8898.
(47) Nguyen, J. Q.; Iverson, B. L. *J. Am. Chem. Soc.* **1999**, *121*, 2639.
(48) Lokey, S. R.; Kwok, Y.; Guelev, V.; Pursell, C. J.; Hurley, L. H.; Iverson, B. L. *J. Am. Chem. Soc.* **1997**, *119*, 7202.
(49) Hunter, C. A.; Lawson, K. R.; Perkins, J.; Urch, C. J. *J. Chem. Soc., Perkin 2* **2001**, 651.
(50) Hill, D. J.; Mio, M. J.; Prince, R. B.; Hughes, T. S.; Moore, J. S. *Chem. Rev.* **2001,** *101*, 3893.
(51) Wright, J. D. *Molecular Crystals*, 2nd ed.; Cambridge University Press: Cambridge, 1995.
(52) Dewar, M. J. S.; Zoebisch, E. G.; Healy, E. F.; Stewart, J. J. P. *J. Am. Chem. Soc.* **1995**, *107*, 3702.
(53) Typically 6−10 molecular orbitals were included in the CI active space.

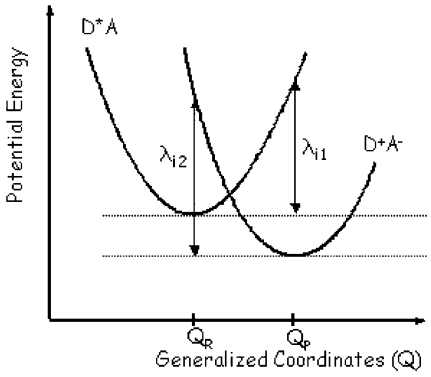


***Figure 14.*** Schematic representation of the reactant (R) and product (P) potential energy curves, with the definition of the reorganization energies $\lambda_{i1}$ and $\lambda_{i2}$ (see text).

respectively; $q_i$ and $q_j$ represent the donor and acceptor partial atomic charges (as provided by a Mulliken population analysis on the basis of the AM1 electronic structure of the singly oxidized and reduced isolated molecules) that are separated by a distance $r_{ij}$ in the $D^+A^-$ state of the whole assembly.

The reorganization energy $\lambda$ includes contributions from the vibrations of the molecules (intramolecular energy $\lambda_i$) and from the polarization change in the solvent environment (solvent reorganization energy $\lambda_s$): $\lambda = \lambda_i + \lambda_s$. The intramolecular reorganization energy ($\lambda_i$) corresponds to the nuclear relaxation energy, i.e., the energy cost when going from the reactant, $Q_R$, to the product, $Q_P$, equilibrium geometry either along the potential energy surface of R ($\lambda_{i1}$) or along that of P ($\lambda_{i2}$) (see Figure 14); different $\lambda_{i1}$ and $\lambda_{i2}$ values are obtained when the R and P parabola have different curvatures, in which case $\lambda_i$ is defined as the average value of $\lambda_{i1}$ and $\lambda_{i2}$[58]

$$\lambda = \frac{1}{2}(\lambda_{i1} + \lambda_{i2}) \tag{6}$$

with

$$\lambda_{i1} = E^{D^*A}(Q_P) - E^{D^*A}(Q_R) \approx \{E^{D^*}(Q_P) + E^{A}(Q_P)\} - \{E^{D^*}(Q_R) + E^{A}(Q_R)\}$$

and

$$\lambda_{i2} = E^{D^+A^-}(Q_R) - E^{D^+A^-}(Q_P) \approx \{E^{D^+}(Q_R) + E^{A^-}(Q_R)\} - \{E^{D^+}(Q_P) + E^{A^-}(Q_P)\}$$

where $E^{D^*}$, $E^{D^+}$, $E^{A}$, and $E^{A^-}$ correspond to the total energy of the isolated donor in its lowest singlet excited and cationic states and that of isolated acceptor in its ground and anionic states, respectively.[59] As is generally assumed, a single effective mode at 0.2 eV (corresponding to the C=C double-bond vibration mode) has been considered to take into account the role of vibrations in assisting the transfer.

The solvent reorganization energy ($\lambda_s$) is derived from the classical dielectric continuum model of Marcus using spherical cavities surrounding the ionized donor and acceptor units. This model assumes that the time scale of the electron-transfer process is much shorter than that associated to the solvent nuclear reorganization. In our approach, $\lambda_s$ also takes into account the spatial distribution of the positive and negative charges by expanding the donor−acceptor interaction in the following way

$$\lambda_s = \frac{1}{8\pi\epsilon_0}\left[\underbrace{\left(\frac{q_D^2}{R_D} + \frac{q_A^2}{R_A}\right)}_{\text{isolated system}} + \underbrace{\left(2\sum_i^{N_D}\sum_j^{N_A}\frac{q_i q_j}{r_{ij}}\right)}_{\text{interaction}}\right]\left(\frac{1}{\epsilon_{op}} - \frac{1}{\epsilon_s}\right) \tag{7}$$

where $q_i$, $q_j$, and $r_{ij}$ have the same meaning as before (note that $\sum_i q_i = q_D$ for the donor and $\sum_j q_j = q_A$ for the acceptor; $\epsilon_{op}$ and $\epsilon_s$ stand for the optical and static dielectric constants of the medium; $R_D$ and $R_A$ are effective spherical cavity radii for the donor and acceptor, respectively). These were estimated from the molecular volumes calculated on the basis of the van der Waals atomic radii and the AM1 molecular geometries; the calculated values amount to 3.91 Å for the PERY chromophore and 4.74 Å for the OPV segment, in reasonable agreement with the values obtained on the basis of the measured densities (4.71 and 5.05 Å, respectively). The first term in eq 7 represents the stabilization of the isolated ions in a continuum dielectric (Born term), while the second term describes Coulombic attraction between the opposite charges (here developed in a multicentric form) in the $D^+A^-$ charge-separated state. Note that the solvent reorganization energies calculated in **M1** using this approach should be considered with caution, owing to the small distance between the positive and negative charges.[60]

The tunneling matrix elements for charge separation and recombination were calculated by means of the generalized two-state Mulliken−Hush model[61] on the basis of an adiabatic description of the reactant and product states

$$V_{RP} = \frac{\mu_{RP}^{ad}\Delta E_{RP}^{ad}}{\sqrt{(\Delta\mu_{RP}^{ad})^2 + 4(\mu_{RP}^{ad})^2}} \tag{8}$$

This expression involves the energy difference ($\Delta E_{RP}^{ad}$) as well as the corresponding dipole moment difference ($\Delta\mu_{RP}^{ad}$) and transition dipole moment ($\mu_{RP}^{ad}$) between R and P. We have computed these parameters in the nuclear arrangement representative of the reactants ($Q_R$) (and without taking into account the solvent effects) by means of the semiempirical Hartree−Fock INDO (intermediate neglect of differential overlap)[62] Hamiltonian coupled to a configuration-interaction scheme

(54) Bixon, M.; Jortner, J. In *Advances in Chemical Physics*; Jortner, J., Bixon, M., Eds.; John Wiley & Sons: New York, 1999; Vol. 106, pp 35−202.
(55) Jortner, J. *J. Chem. Phys.* **1976**, *64*, 4860
(56) Klamt, A.; Schürmann, G. *J. Chem. Soc., Perkin Trans.* **1993,** *2*, 799.
(57) Ampac 6.55 ed.; Semichem: 7204 Mullen, Shawnee, KS 66216, 1997.
(58) Pourtois, G.; Beljonne, D.; Cornil, J.; Ratner, M. A.; Brédas, J. L. *J. Am. Chem. Soc.* **2002**, *124*, 4436.
(59) Owing to the limited number of molecular orbitals used in the configuration interaction expansion, the CAS-CI approach used for the geometry optimizations provides an unbalanced treatment of electron correlation effects in the ground state and excited states leading to overestimated excitation energies. To overcome this problem, the energies of the electronic states involved in the determination of $\lambda_i$ and $\Delta G°$ were calculated by retaining only singly excited configurations in the CI scheme, which allows for correlation effects in a more size-consistent way and provides transition energies in better agreement with experiment
(60) Though we stress that eq 7 is already an improvement over the standard formulation that simply considers the interaction between point charges located at the centers of the donor/acceptor moieties, such a simplified model would lead to negative reorganization energies for small−as compared to the donor and acceptor radii−donor−acceptor interdistances
(61) Cave, R. J.; Newton, M. D. *Chem. Phys. Lett.* **1996,** *15*, 249
(62) Ridley, J.; Zerner, M. C. *Theor. Chim. Acta* **1973**, *32*, 111.

***Table 3.*** Molecular Parameters Involved in the Calculation of the Charge Separation and Charge Recombination Rates, Following Eq 4[a]

| process | $\lambda_i$ (eV) | $\lambda_s$ (eV) | $V_{RP}$ ($cm^{-1}$) | $\Delta G°$ (eV) | $k_{RP}$ ($ns^{-1}$) |
|---|---|---|---|---|---|
| | | | M1 | | |
| $D^*A \rightarrow D^+A^-$ | 0.22 | 0.05 | 435 (570) | −1.1 | 451 (770) |
| $DA^* \rightarrow D^+A^-$ | 0.31 | 0.04 | 65 (71) | −1.0 | 84 (100) |
| $D^+A^- \rightarrow DA$ | 0.45 | 0.04 | 177 (190) | −1.6 | 43 (50) |
| | | | P2 | | |
| $D^*A \rightarrow D^+A^-$ | 0.25 | 0.08 | 9.2 | −0.6 | 10 |
| $DA^* \rightarrow D^+A^-$ | 0.31 | 0.08 | 8.0 | −0.6 | 7 |
| $D^+A^- \rightarrow DA$ | 0.45 | 0.08 | 11.6 | −2.1 | 0.007 |

[a] $\lambda_i$ and $\lambda_s$ are the internal and external reorganization energies, respectively, and $\Delta G^0$ is the change in free Gibbs energy. The numbers between parentheses have been obtained on the basis of the DA ground-state geometry, see text.

involving single excitations (SCI) with respect to the Hartree−Fock determinant.

The calculated electronic couplings, $V_{RP}$, are found to depend critically on the molecular geometry (face-to-face versus extended structures, donor−acceptor separation, torsion angle between donor and acceptor, relative orientations of the chromophores, etc.) and on the nature of the initial excited state (D*A versus DA*). The $V_{RP}$ values computed at the INDO/SCI level using the relaxed geometries in the reactant state (e.g., the geometries of the donor excited state and acceptor ground state for D*A) are listed in Table 3 for direct and indirect charge transfer and charge recombination together with the corresponding couplings estimated on the basis of the neutral ground-state (DA) geometry. The two sets of $V_{RP}$ values are close, which indicates that, in most cases, the Franck−Condon approximation holds reasonably well, i.e., the amplitude of the electronic tunneling matrix elements is weakly dependent on the geometric structure used as input for the calculation.[63]

From Table 3 it is seen that the electronic couplings are much larger in the case of the **M1** cyclic molecule than the **P2** extended structure for both charge separation and recombination. As pointed out previously, the higher electronic couplings obtained for **M1** are consistent with stronger interactions when the two chromophores are in a cofacial arrangement. The molecular mechanics calculations suggest almost parallel orientations for the donor and acceptor moieties in the cyclic structure; however, the measured CD spectrum (Figure 3) indicates a chiral arrangement of the OPV and PERY units. We have thus repeated the electronic coupling calculations by imposing an angle between the donor and acceptor molecular axes from 0° to 40° (i.e., a range of angles still compatible with the closed structure of the macrocycle) and found no significant difference.

The relative magnitude of the electronic couplings can be gauged qualitatively from an inspection of the frontier molecular orbitals that participate in the description of the relevant electronic states, Figure 15. For efficient charge transfer, the donor and acceptor orbitals have to fulfill two criteria:[64] (i) they should lie close in energy and (ii) they should lead to significant overlap between the corresponding wave functions, a characteristic that depends critically on symmetry and spatial confinement.

In that context, we note that the molecular architecture of **P2** is such that the perylene bisimides are covalently linked to the OPV segments via their nitrogen atoms; this is far from being optimal for photoinduced hole or electron migration since both the HOMO and LUMO levels of the perylene derivatives display nodes on these nitrogen atoms, thus impeding efficient communication between the chromophores. From a detailed analysis of the transition dipole moments that provide the dominant contribution to the electronic coupling, we have identified deeper lying molecular orbitals as the main contributors to the charge separation process in **P2** and **M1**. Some of these MOs are shown in Figure 15. For instance, for electron transfer, the LUMO+2 level of PERY has the appropriate symmetry and energy to interact with the LUMO level of OPV in both the head-to-tail arrangement of **P2** and, even more strikingly, the cofacial architecture of **M1**. Indeed, the LUMO+2 orbital of PERY is symmetric with respect to the mirror plane perpendicular to the molecular frame, which is also the case for the LUMO orbital of OPV when focusing on the individual phenylene rings (the mirror plane corresponds in this case to the plane perpendicular to each aromatic ring and passing through the carbon atoms in para positions). The large contributions of the PERY HOMO-4 and OPV HOMO-6 to the electronic couplings for hole transfer can be rationalized on the basis of similar symmetry arguments. (A detailed analysis of these intriguing symmetry effects, which have been elegantly described by Verhoeven,[65] together with molecular engineering strategies for the design of improved materials will be described elsewhere[66]).

The thermodynamics parameters together with the resulting charge separation and charge recombination rates, as calculated when considering toluene as the solvent ($\epsilon_s = 2.38$), are also collected in Table 3. For both compounds, the relaxation energies $\lambda_i$ are larger for charge recombination than for charge separation. This is expected since the donor ionized state geometry resembles more the excited-state geometry than the ground-state geometry. We note that $\lambda_i$ is slightly larger for charge separation from the excited acceptor, pointing out to a larger geometric difference in the perylene derivative. The main contribution to $\lambda_i$ then arises from the reduction of the electron-withdrawing unit. The solvent reorganization energy $\lambda_s$ is in all cases small due to the low dielectric constant of the solvent; in addition, the close proximity of the positive and negative charges in **M1** further reduces the solvent-induced stabilization (the charges are strongly bound within the molecular structure).

The driving force, $\Delta G°$, is calculated to be negative in both systems (confirming that the charge separation is an exergonic process) and significantly smaller for **P2** than **M1**, as a result of the strong interaction between the positive and negative charges in the cyclic structure (which stabilizes the charge-separated state). Quantitatively, the $\Delta G°$ values are markedly different from those obtained from the Weller equation (eq 1), Table 1. The reason for this discrepancy lies mainly in the second term of eq 1, i.e., the Coulomb attraction between the

(63) We note, however, a significant difference between the values calculated using the two geometries for the electron-transfer process from the donor to the acceptor ($D^*A \rightarrow D^+A^-$) in **M1**, a feature which is due to significant mixing between donor and acceptor excited-state wave functions when allowing the OPV geometry to relax.

(64) Beljonne, D.; Pourtois, G.; Ratner, M. A.; Brédas, J. L. Submitted for publication.

(65) See, for instance: Verhoeven, J. W. In *Advances in Chemical Physics*; Jortner, J., Bixon, M., Eds.; John Wiley & Sons: New York, 1999; Vol. 106, pp 603−644.

(66) Dupin, H.; et al. Manuscript in preparation.

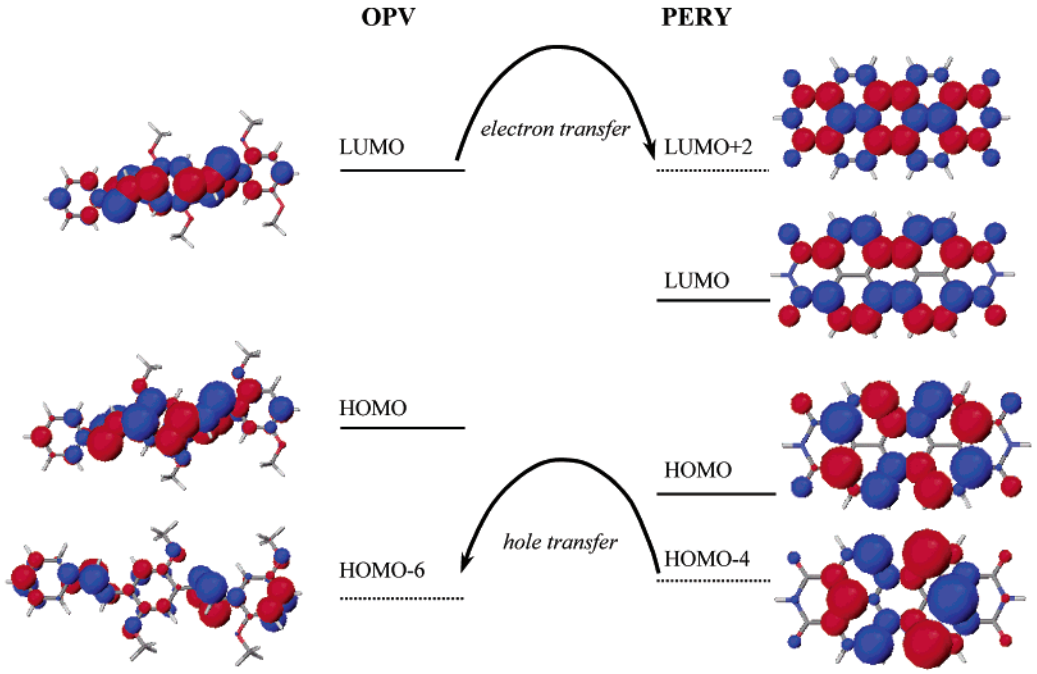


***Figure 15.*** Schematic energy diagram showing the frontier molecular orbitals of the OPV and PERY chromophores, as obtained at the INDO level. Arrows represent the pathways that provide the main contributions to the electronic couplings (see text).

positive and negative charges. While a point-charge model is assumed in eq 1, a more reliable estimate of this Coulomb interaction is obtained using eq 5, which takes into account the actual charge distributions along the donor/acceptor chromophores (polarization effects, accounted for in the quantum-chemical calculations, lead to the appearance of positive and negative partial charges alternating along the conjugated pathway and reduce the overall interaction between the opposite charges, especially in **M1**). When correcting eq 1 for these effects (i.e., injecting the calculated Coulomb binding energies in eq 1 while keeping the experimental results for the other terms), the changes in Gibbs free energy for direct charge separation (induced by exciting the OPV segment) are ca. −0.9 and −0.4 eV for **M1** and **P2**, respectively, in excellent agreement with the values in Table 3 (−1.1 and −0.6 eV, respectively).

We are now in a position to discuss the overall rates for charge separation and charge recombination. The latter process in **P2** and, to a lesser extent, **M1** involves a very large driving force (see Table 3), corresponding to the 'inverted' regime in Marcus theory (for $|\Delta G^\circ| \gg \lambda$, the rate decreases with increasing driving force). For charge separation, $|\Delta G^\circ|$ in **P2** is close to the total reorganization energy, while in **M1** $|\Delta G^\circ|$ is significantly greater than $\lambda$. Therefore, the activation barrier for photoinduced charge transfer is smaller in **P2** than in **M1**, which partly counteracts the larger electronic tunneling matrix elements computed for the cyclic structure. The calculated transfer rates are consistent with this qualitative analysis, with about 1 order of magnitude enhancement in the charge separation rates calculated for **M1** with respect to **P2** and larger rates for charge separation in comparison to recombination (especially in the case of **M1**). We further note that the electron-transfer process is predicted to be much more efficient than hole transfer in **M1** while they display similar rates in **P2**. These trends are fully consistent with the experimental results in Table 2; however, there are significant deviations between the measured and calculated rates as a result of the high sensitivity of the rates on the electronic couplings and mostly the various thermodynamical parameters involved in the exponential function of eq 4.

## Conclusions

Two new copolymers (**P1** and **P2**, Figure 1) consisting of alternating OPV donor and PERY acceptor segments have been synthesized using a palladium-catalyzed Suzuki reaction. Additionally, a cyclic compound **M1** in which the two chromophores are in a face-to-face orientation could be isolated from the polymerization of **P1**. Excitation of either of the chromophores in **P1**, **P2**, or **M1** results in photoinduced energy- and electron-transfer reactions. Photoluminescence quenching, photoluminescence lifetime, and transient pump−probe spectroscopy have been used to assess rates for energy transfer ($k_{et}$), direct and indirect charge separation ($k_{cs}^{d}$ and $k_{cs}^{i}$), and charge recombination ($k_{rec}$) of these materials in solution and in thin films (Figure 6, Table 2). The direct forward electron transfer, i.e., from OPV($S_1$), is extremely fast ($k_{cs}^{d} \geq 3.5 \times 10^{11}$ $s^{-1}$) for all systems but especially high in the case of **M1**. The rate for singlet energy transfer from OPV($S_1$) to PERY($S_1$) is competitive with the fast direct charge separation. The recombination rates vary more strongly with the sample (Table 2). The longest lifetimes (0.5−1.6 ns) are observed for **P1** and **P2** in toluene. Quantum-chemical calculations confirm that higher rates are obtained in **M1** with respect to **P2**; this mostly comes from a larger electronic coupling due to the strong donor−acceptor interactions in the face-to-face arrangement of the macrocyclic compound. The calculations point to the very strong dependence of the electronic couplings between donor and acceptor, on molecular orientations (geometries), orbital symmetries and energies, and the nature of the initial excited state.

In the films, geminate recombination is much faster, although some charges are able to diffuse away and are longer lived. Polymers **P1** and **P2** have been tested in photovoltaic devices.

Working cells with satisfactory open-circuit voltages ($V_{OC}$ = 1−1.2 V) were prepared, but the short-circuit current densities ($J_{SC}$ = 0.008−0.012 mA cm$^{-2}$) under AM1.5 conditions were extremely low. The low currents likely result from fast geminate recombination (more than 80% recombination in the first ns) and poor transport characteristics due to face-to-face orientations of OPV and PERY segments in alternating stacks in the polymer films.

The photophysical results on **P1** and **P2** provide an important guideline for design of new alternating copolymers that could be more effective in polymer photovoltaic cells. To overcome the intrinsic tendency of donor and acceptor segments to give alternating stacks (Figure 13), stronger antagonistic interactions that direct the microscopic morphology should be introduced. This might be accomplished by using segments that differ more strongly in size, or by utilizing the low entropy of mixing (e.g., in block copolymers), or by introducing anchoring points at the polymer chains (e.g., via interchain hydrogen bonds) that secure the relative positions of donor and acceptor. Because charge separation is slower for an end-to-end substitution of the two chromophores (as in **P2)** than for a face-to-face orientation (as in **M1**), care must be taken that the rate of electron transfer remains high enough to guarantee efficient charge generation in these desired isolated neighboring stacks of donors and acceptors. Current investigations are directed toward such appealing systems.

## Experimental Section

**Synthesis.** The detailed experimental procedures for the synthesis and characterization of the compounds **1**−**13**, **M2**, **M3**, **P1,** and **P2** are given in the Supporting Information.

**General Methods.** Cyclic voltammograms were measured in 0.1 M tetrabutylammonium hexafluorophosphate ($TBAPF_6$) as a supporting electrolyte in dichloromethane using a Potentioscan Wenking POS73 potentiostat. The working electrode was a Pt disk (0.2 cm$^2$), the counter electrode was a Pt plate (0.5 cm$^2$), and a saturated calomel electrode (SCE) was used as the reference electrode, calibrated against $Fc/Fc^+$ (+0.43 V). UV−vis absorption spectra were recorded on a Perkin-Elmer Lambda 900 spectrophotometer. Fluorescence spectra were recorded on an Edinburgh Instruments FS920 double-monochromator spectrometer and a Peltier-cooled red-sensitive photomultiplier.

**Fluorescence Lifetimes.** Time-correlated single-photon counting fluorescence studies were performed using an Edinburgh Instruments LifeSpec-PS spectrometer, consisting of a 400 nm picosecond laser (PicoQuant PDL 800B) operated at 2.5 MHz and a Peltier-cooled Hamamatsu microchannel plate photomultiplier (R3809U-50). Lifetimes were determined from the data using the Edinburgh Instruments software package.

**Photoinduced Absorption Spectroscopy.** Near steady-state photoinduced absorption (PIA) spectra were recorded between 0.25 and 3 eV by exciting a thin drop-cast film on quartz in an Oxford Optistat continuous flow cryostat with a mechanically modulated (typically 275 Hz) cw Ar-ion laser (Spectra Physics 2025) pump beam tuned to 458 or 528 nm (25 mW, beam diameter of 2 mm) and monitoring the resulting change in transmission ($\Delta T$) of a tungsten−halogen white-light probe beam after dispersion by a triple-grating monochromator, using Si, InGaAs, and (cooled) InSb detectors.

The femtosecond laser system used for pump−probe experiments consists of an amplified Ti-sapphire laser (Spectra Physics Hurricane), providing 150 fs pulses at 800 nm with an energy of 750 $\mu$J at 1 kHz. Pump (450 or 520 nm, fluence 0.5 $\mu$J/mm$^2$) and probe (1450 nm) pulses were created by optical parametric amplification and 2-fold frequency doubling using two OPAs (Spectra Physics OPA-C). The pump beam was linearly polarized at the magic angle (54.7°) with respect to the probe beam. The temporal evolution was recorded using an InGaAs detector and standard lock-in detection at 500 Hz.

**Photovoltaic Cells.** For fabrication of devices, polyethylenedioxythiophene polystyrenesulfonate (PEDOT:PSS, Bayer AG) was spin coated from an aqueous dispersion under ambient conditions on precleaned (washing, UV ozone treatment) ITO covered glass substrates, and the layer was dried by annealing the substrate on a hot plate. The resulting PEDOT:PSS film thickness is about 100 nm. The polymers **P1** and **P2** were spin cast from chloroform to give an active layer of ∼100 nm thickness as determined with a Tencor P10 surface profiler. Finally, a LiF(1 nm)/Al(100 nm(back electrode was deposited by thermal evaporation under vacuum ($5 \times 10^{-6}$ mbar, 1 ppm $O_2$ and <1 ppm $H_2O$). The active area of the device is 0.1 cm$^2$. Illumination was performed with a Steurnagel SolarConstant 1200 solar simulator, set to 100 mW cm$^{-2}$.

**Acknowledgment.** We thank Edwin H. A. Beckers for assistance in the pump−probe experiments. The Eindhoven-Mons collaboration is supported by the European Commission, under the RTN network 'LAMINATE'. The research in Eindhoven has been supported by the Netherlands Organization for Chemical Research (CW), the Netherlands Organization for Scientific Research (NWO), and the Eindhoven University of Technology through a grant in the PIONIER program. The work at Arizona is partly supported by the National Science Foundation, the Office of Naval Research, and the IBM Shared University Research Program. The work in Mons is partly supported by the Belgian Federal Services for Scientific, Technical, and Cultural Affairs (InterUniversity Attraction Pole 5/3) and the Belgian National Science Foundation (FNRS). David Beljonne and Jérôme Cornil are Research Associates from FNRS. The research of S. C. J. Meskers has been made possible by a fellowship of the Royal Netherlands Academy of Arts and Sciences.

**Supporting Information Available:** Experimental procedures for the synthesis and characterization of compounds. This material is available free of charge via the Internet at http://pubs.acs.org. See any current masthead page for ordering information and Web access instructions.

JA034926T